A Multiple-Winding Magnetics Model Having Directly Measurable Parameters

Robert W. Erickson and Dragan Maksimovic
Colorado Power Electronics Center
University of Colorado, Boulder, 80309-0425
rwe@boulder.colorado.edu maksimov@colorado.edu
http://ece-www.colorado.edu/~pwrelect

***Abstract* — A general model of the multiple-winding transformer and coupled inductor is presented, in which all parameters can be directly measured. The approach is suitable for all winding geometries, and simplifying approximations can be easily made. This model can be applied in determination of cross-regulation, current ripple, and small-signal dynamics of multiple-output dc-dc converters. An experimental four-winding flyback transformer example is investigated. Observed leakage inductance parameter measurements are interpreted physically, and are related to observed flyback converter waveforms. It is also shown that the model correctly predicts small-signal dynamics.**

1. Introduction

In comparison with modeling of single-output converters, the current state of knowledge regarding multiple-output converters is poor. Averaging techniques have been used to model how conduction losses affect cross-regulation [1-4]. The magnetics of multiple-output converters generally contain several windings having moderate to good coupling. Cross regulation of these converters is usually dominated by transformer leakage phenomena. Effects of leakage inductance and coupled inductors on cross regulation of forward converters are described in [5-7], and cross regulation in the discontinuous conduction mode flyback converter is analyzed in [8,9]. Nonetheless, the effects of coupling between magnetics windings on converter behavior have not been adequately modeled. Better understanding and modeling of the various continuous and discontinuous conduction modes, winding current ripples, output voltage cross regulation mechanisms, and small-signal dynamic phenomena is needed.

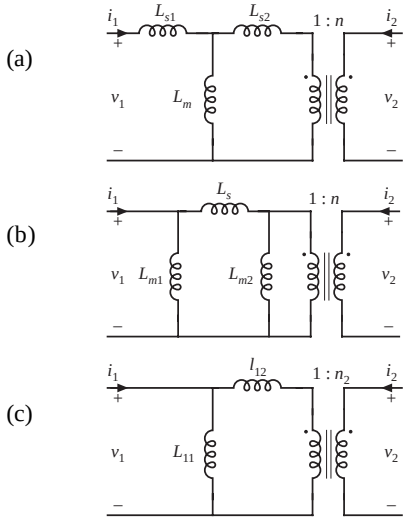

Fig. 1. Well-known two-winding transformer models: (a) T, (b) pi, (c) cantilever.

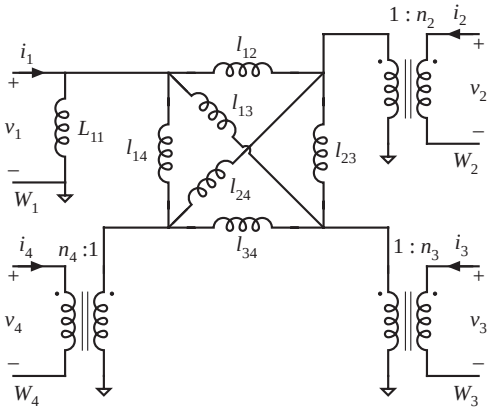

Fig. 2. Extended cantilever model, four-winding example.

Of central importance to this problem is the modeling of the multiple-winding transformer. Transformer modeling is an old and well-understood process, yet in modern practice a number of problems are often encountered. The model may not be sufficiently general to correctly predict observed converter behavior. The model may be so complicated that it leads to intractable results. Computations may be numerically ill-conditioned. Determination of the values of model parameters can be difficult in practice, unless each parameter can be independently measured. The intent of this paper is to select and review transformer modeling techniques appropriate to the multiple-output converter problem, and to show how these models correctly predict observed waveforms and converter behavior.

Several authors have attacked the problem of modeling multiple-winding dc-dc converter magnetics through the use of reduced-order models based on the physical winding geometry [10-15]. The benefits of this approach are the relative simplicity of the model and the availability of approximate analytical expressions for the leakage inductance parameters. One disadvantage of this approach is its lack of generality; for example, it cannot be easily applied to toroidal geometries. Another disadvantage is its lack of accuracy: reduced-order models cannot correctly predict all possible winding waveforms for all possible excitations. Both disadvantages are

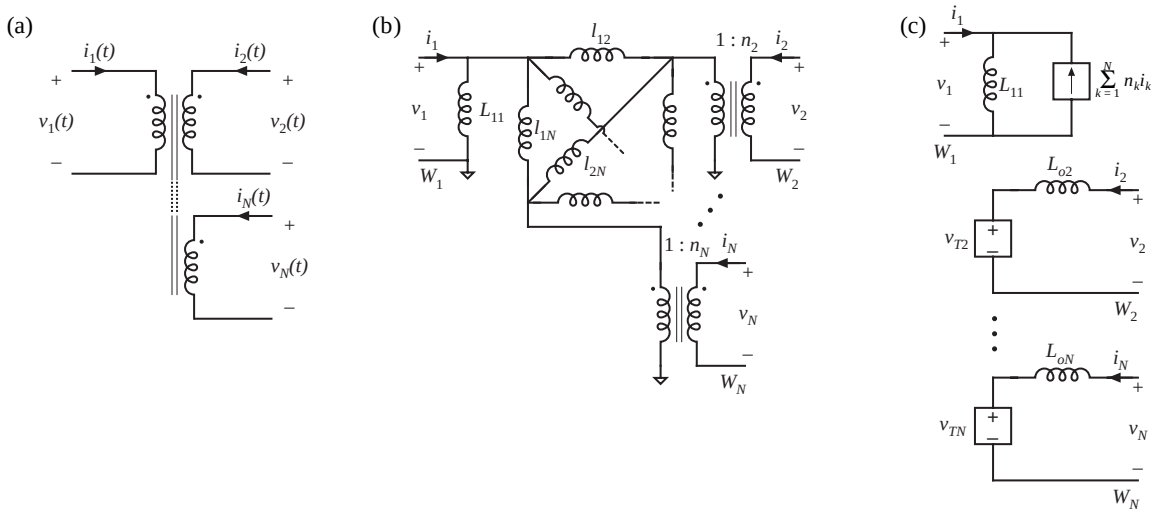

Fig. 3. An *N*-winding transformer (a), its extended cantilever model (b), and its *N*-port model (c).

apparently significant in the multiple-output cross regulation problem.

Figure 1 illustrates three well-known equivalent circuit models for the two-winding transformer. The T model cannot be directly generalized to *N* windings—the simple transformer model containing one leakage inductance per winding is insufficient to describe the behavior of transformers containing more than three windings [10,11]. In general, $N(N + 1)/2$ independent parameters are required to model a transformer containing *N* windings. On the other hand, the pi model can indeed be generalized to the *N* winding case; the result is known as the "link" model [11]. The link model contains $(N - 1)$ extra parameters, and hence is underdetermined. The tight coupling common in multiple-output converter transformers causes the link model to be numerically ill-conditioned, and determination of the values of the shunt inductances is difficult.

The well-known cantilever model of Fig. 1 [16] can also be generalized to the *N* winding case. A four-winding example is illustrated in Fig. 2. This model contains the correct number of independent parameters. It is well-suited for modeling the closely-coupled transformers of multiple-output converters because each parameter can be directly measured, and because there is only one shunt inductance. Section 2 contains a physical explanation of the extended cantilever model, including how to directly measure each model parameter. The close relationship between the extended cantilever model and the inverse inductance matrix is also described. Section 3 illustrates the connection between the extended cantilever model and the *N*-port hybrid parameter transformer model. This *N*-port model can be better suited to computer simulation since the number of inductors is equal to the number of independent states, and hence there are no inductor-only loops.

A three-output flyback converter was constructed and modeled. In Section 4, the measured extended cantilever model of the four-winding flyback transformer is given. Simulations incorporating this model are able to correctly predict the converter waveforms, including (1) how some outputs may operate in discontinuous conduction mode while others operate in continuous conduction mode, (2) output voltage cross regulation, and (3) the positive and negative slopes of the winding currents. Indeed, the extended cantilever model explains the mechanisms of cross regulation in the flyback converter.

The small-signal dynamics of the three-output flyback converter were also predicted using the *N*-port model. The control-to-output transfer function of the main CCM output changes significantly when auxiliary outputs enter the discontinuous conduction mode. The *N*-port model, in conjunction with the automated small-signal analysis approach of [18], was found to easily predict the system dynamics; good agreement between experimental data and theoretical models was obtained.

Conclusions are summarized in Section 5.

2. The Extended Cantilever Model

The extended cantilever model of Fig. 2 contains a single shunt inductance L_{11} that models the self-inductance of winding W_1. The effective turns ratios n_2, n_3,... are equal to the ratios of the actual winding voltages, under open-circuit conditions. These effective turns ratios are not in general equal to the physical turns ratios because, when leakage flux is present, different total fluxes may link the windings. In addition, the model contains an effective leakage inductance l_{jk} connected between each winding.

Each parameter of the extended cantilever model can be directly measured, as follows. The self-inductance L_{11} is measured in the usual manner, by open-circuiting windings W_2, W_3,..., and measuring the inductance of winding W_1. To measure the effective turns ratios n_2, n_3,..., a voltage is applied to winding W_1 with the other windings open-circuited. The effective turns ratio n_k is given by

$$n_k = \frac{v_k}{v_1} \tag{1}$$

A negative value of n_k indicates that the winding polarity marks should be reversed.

To measure the effective leakage inductance l_{jk}, winding W_j is driven with voltage source v_j, while all other windings are short-circuited. It is important that good low-impedance short-circuits be used. The current i_k in winding W_k is measured. The effective leakage inductance l_{jk} is given by

$$l_{jk} = \frac{v_j(s)}{s n_j n_k i_k(s)} \tag{2}$$

with n_1 taken to be equal to 1, and where s is the Laplace transform operator. It is possible for l_{jk} to be negative; hence, polarities must be carefully observed.

Note that the problem of the small difference of large numbers is avoided, complex calculations are not necessary, and each parameter is measured directly. A complete model can be easily determined, without need to resort to approximate physical arguments. If desired, a reduced-order model can be obtained by open-circuiting large leakage inductances, short-circuiting small leakage inductances, etc.

The parameters of the extended cantilever model are closely related to the elements of the inverse inductance matrix. Given the inductance matrix **L**, inverse inductance matrix **B**, and vectors **v** and **i** containing the winding voltages and currents, respectively, one can write the following equations:

$$\begin{aligned} &\mathbf{v} = s\mathbf{L}\mathbf{i} \\ &\mathbf{L} = \left\langle L_{jk} \right\rangle \quad \textit{inductance matrix} \\ &\mathbf{B} = \mathbf{L}^{-1} = \left\langle b_{jk} \right\rangle \quad \textit{inverse inductance matrix} \end{aligned} \tag{3}$$

The parameters of the extended cantilever model are then given by

$$\begin{aligned} L_{11} &= L_{11} \\ n_j &= \frac{L_{1j}}{L_{11}} \\ l_{jk} &= -\frac{1}{n_j n_k b_{jk}} \end{aligned} \tag{4}$$

Conversely, the elements of the inverse inductance matrix can be expressed in terms of the extended cantilever model parameters as

$$\begin{aligned} b_{jk} &= -\frac{1}{n_j n_k l_{jk}}, \quad j \neq k \\ b_{jj} &= \frac{1}{n_j} \sum_{k=1}^{N} \frac{1}{l_{kj}}, \quad \text{with } l_{jj} = \begin{cases} \infty \text{ if } j \neq 1 \\ L_{11} \text{ when } j = 1 \end{cases} \end{aligned} \tag{5}$$

It can be concluded that the extended cantilever model is both valid and general in the N-winding case.

3. The N-Port Model

The extended cantilever model is also closely related to an N-port description of the transformer. Indeed, the parameter measurements described in Section 2 amount to measurements of the N-port parameters of the transformer; hence, transformation between the extended cantilever model of Fig. 3(b) and the N-port model of Fig. 3(c) is simple and direct. This N-port description is useful in deriving expressions for current ripples and the zero-ripple condition [7].

In this N-port model, the primary winding is modeled by its current-controlled Norton equivalent network as shown in Fig. 3(c). The inductance of this port is the primary self-inductance L_{11}. The current-controlled current source is equal to the sum of the secondary winding currents, each transferred through their respective effective turns ratios.

Each secondary winding is modeled by a voltage-controlled Thevenin equivalent network. The series inductance of winding k, L_{ok}, is equal to the parallel combination of all effective leakage inductances connected to winding k, and reflected through the turns ratio n_k:

$$L_{ok} = n_k^2 \left(l_{1k} \| l_{2k} \| \cdots \| l_{(k-1)k} \| l_{(k+1)k} \| \cdots \| l_{Nk} \right) \tag{6}$$

The voltage-controlled voltage source is given by

$$\begin{aligned} v_{Tk} = &\frac{L_{ok}}{n_k l_{1k}} v_1 + \frac{L_{ok}}{n_k n_2 l_{2k}} v_2 + \cdots + \frac{L_{ok}}{n_k n_{k-1} l_{(k-1)k}} v_{k-1} \\ &+ \frac{L_{ok}}{n_k n_{k+1} l_{(k+1)k}} v_{k+1} + \cdots + \frac{L_{ok}}{n_k n_N l_{Nk}} v_N \end{aligned} \tag{7}$$

Each coefficient in Eq. (7) is the voltage gain between two windings, when all other windings are short-circuited.

Zero ripple occurs in winding k when

$$v_{Tk} = v_k \tag{8}$$

This zero ripple condition is described further in [7].

The N-port model is useful in computer simulations, because it avoids the inductor-only loops of the extended cantilever model. Hence, simulation programs such as PSPICE are able to compute the circuit dc operating point. The number of inductors in this model coincides with the number of independent states.

4. Flyback Transformer Example

A simple multiple-output flyback converter was constructed, for the following application:

Input: 30 V (winding W_1)
Output: +12 V (winding W_2)
Output: –12 V (winding W_3)
Output: +3.3 V (winding W_4) (9)

A ferrite EC41-3C80 core was employed, having a 20 mil (0.5 mm) air gap in each leg. The winding configuration is illustrated in Fig. 4.

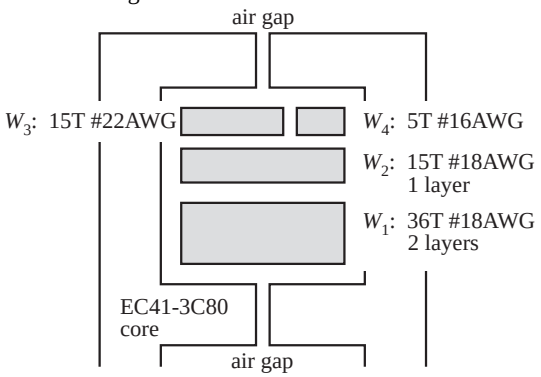

Fig. 4. Winding geometry, Flyback transformer example

4.1 Measurements and model

Measurements of the extended cantilever model parameters were made as described in Section 2. The results are summarized in Table 1. Each leakage inductance parameter was measured in two different ways: as l_{jk} and as l_{kj}. In each case, consistent results were obtained. These measurements lead to the extended cantilever model of Fig. 5.

Table 1. Summary of flyback transformer parameter measurements

parameter	*measured value*
n_2	0.4165
n_3	0.4154
n_4	0.1402
L_{11}	220 µH
l_{12}	4.5 µH
l_{13}	14 µH
l_{14}	130 µH
l_{23}	34 µH
l_{24}	13 µH
l_{34}	–35 µH

Table 2. Flyback transformer output impedance measurements

winding	*measured inductance*	*prediction of model*
W_1	3.0 μH	3.2 μH
W_2	0.48 μH	0.52 μH
W_3	2.3 μH	2.3 μH
W_4	0.31 μH	0.36 μH

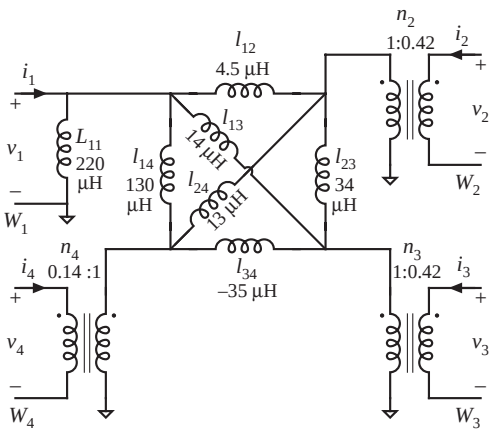

Fig. 5. Extended cantilever model, flyback transformer example

As an additional check, the output impedance of each winding was measured, with all other windings shorted. The measured results are compared in Table 2 with the predictions of the model of Fig. 5 and Eq. (6). It can be seen that agreement is good.

The leakage inductance parameter l_{34} is negative in this example. This parameter relates the voltage driving winding W_3 to the current that flows in winding W_4, when windings W_1, W_2, and W_4 are shorted. Figure 6 illustrates the directions of the winding currents under these conditions. The negative value of l_{34} indicates reversal of the polarity of the induced current I_4.

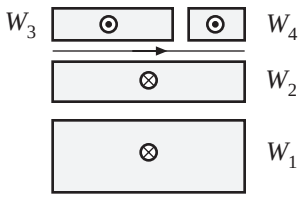

Fig. 6. Direction of leakage flux and induced winding currents, when winding W_3 is driven and windings W_1, W_2, and W_4 are shorted.

Based on the physical winding geometry, one might expect that winding W_1 would be coupled much better to winding W_2 than to windings W_3 and W_4. This explains the relative values of the leakage inductance parameters l_{12}, l_{13}, and l_{14}.

The parameters of the N-port model of the flyback transformer can now be calculated as described in Section 3. The result is diagrammed in Fig. 7.

4.2 Flyback converter behavior

The flyback transformer of Fig. 4 was used in the 100 kHz flyback converter of Fig. 8. This converter operates with the nominal voltages specified in Eq. (9). A voltage-clamp snubber is connected across the primary winding, having an essentially dc voltage V_s.

Secondary winding current measurements are illustrated in Fig. 9(a). It can be seen that the +12V winding (W_2) operates in continuous conduction mode,

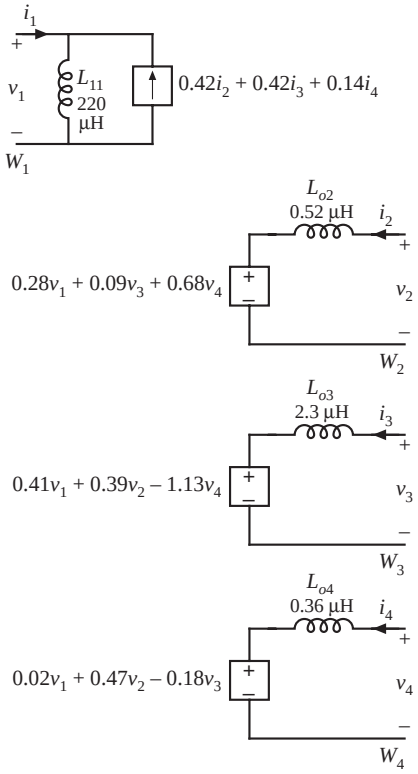

Fig. 7. N-port model parameters, four-winding flyback transformer example

with current ripple having negative slope as would normally be expected. However, the –12V winding (W_3) operates in discontinuous conduction mode. Moreover, the +3.3V winding (W_4) exhibits current ripple having positive slope, opposite of what one might normally expect.

The model of Fig. 5 was implemented in a computer simulation of this flyback converter, using the simulation program PETS [17]. Nonidealities such as MOSFET switching times, diode reverse recovery, and capacitor esr were not modeled. Simulated winding current waveforms are given in Fig. 9(b), for the same operating point described above. It can be seen that agreement is quite good, and the model is able to predict the observed converter behavior. Moreover, it can be concluded that the behavior of multiple-output flyback converters is dominated by the transformer leakage inductances.

The waveforms of Fig. 9 can be easily explained in terms of the extended cantilever model. When the MOSFET turns off, the primary-side snubber diode turns on,

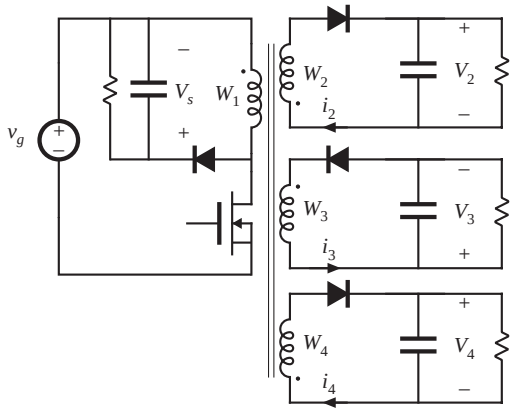

Fig. 8. Flyback converter example

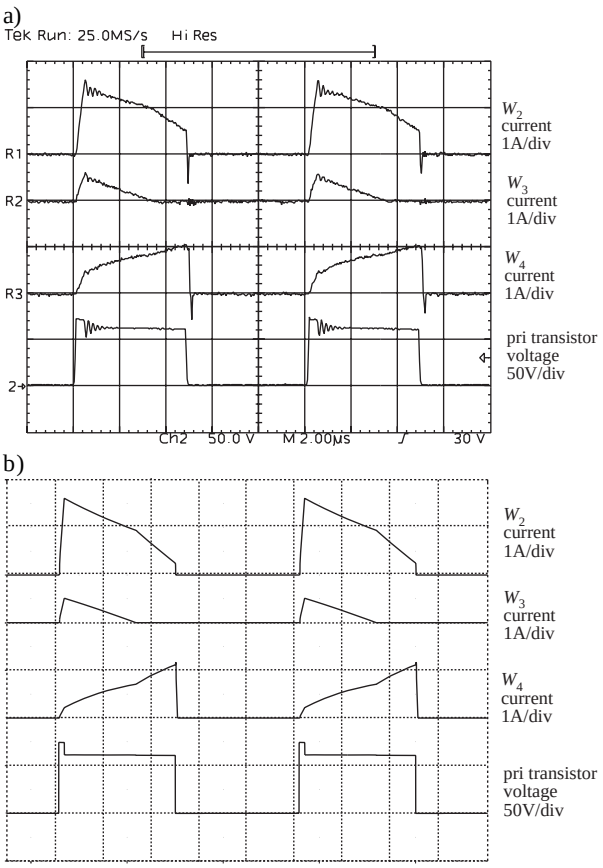

Fig. 9 Comparison of (a) measured, and (b) simulated, waveforms for the flyback converter example.

conducting the magnetizing current and clamping the primary voltage to V_s. The secondary-side diodes also begin conducting. Voltages v_{12}, v_{13}, and v_{14} are applied across the effective leakage inductances l_{12}, l_{13}, and l_{14}, respectively; these voltages are essentially equal and are given by the snubber voltage V_s plus the reflected load voltage. Hence the secondary winding currents increase at rates determined by l_{12}, l_{13}, and l_{14}; these rates are not directly related to the individual load currents.

When the sum of the reflected secondary currents becomes equal to the magnetizing current, then the primary snubber diode turns off. The values of the individual winding currents at this time are determined by the relative values of l_{12}, l_{13}, and l_{14}, and again are not directly related to the individual load currents. During the remainder of the switching period, the secondary winding currents increase or decrease at rates that depend on the differences between the reflected load voltages. The dc load currents must equal the respective average winding currents; hence, increasing the dc load current of a given output requires increasing the slope of its respective winding current. This then implies that the output voltage is reduced. Therefore, each output exhibits a nonzero output resistance, even in continuous conduction mode.

It can be concluded that modeling of transformer leakage inductance parameters is the key to understanding the behavior of multiple output flyback converters.

4.3. Small-signal dynamics

The extended cantilever model is also able to correctly predict converter small-signal dynamics. Of particular interest is the substantial change that occurs in the control-to-main-output transfer function when auxiliary outputs change between continuous conduction and discontinuous conduction. Prediction of observed laboratory behavior requires that the transformer be correctly modeled.

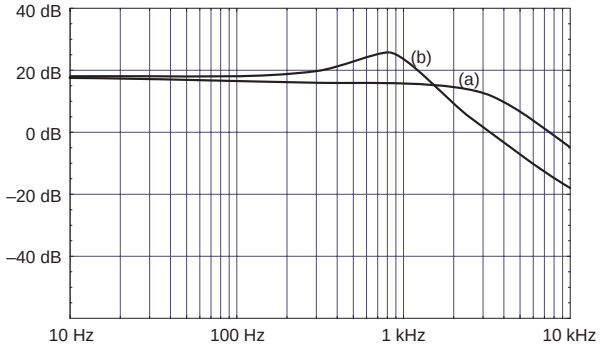

Fig. 10. Predicted CCM duty-cycle-to-W_4-output transfer function magnitude: (a) with W_2 and W_3 outputs operating in DCM, (b) with W_2 and W_3 outputs operating in CCM.

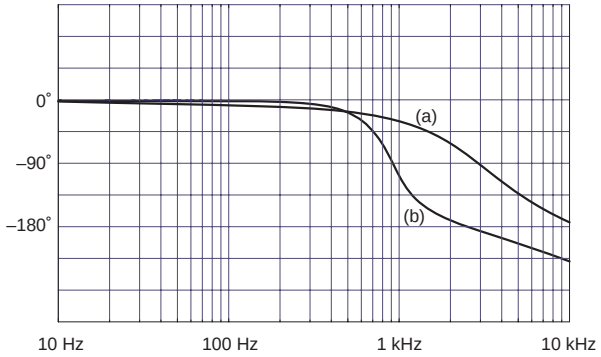

Fig. 11. Predicted CCM duty-cycle-to-W_4-output phase response: (a) with W_2 and W_3 outputs operating in DCM, (b) with W_2 and W_3 outputs operating in CCM.

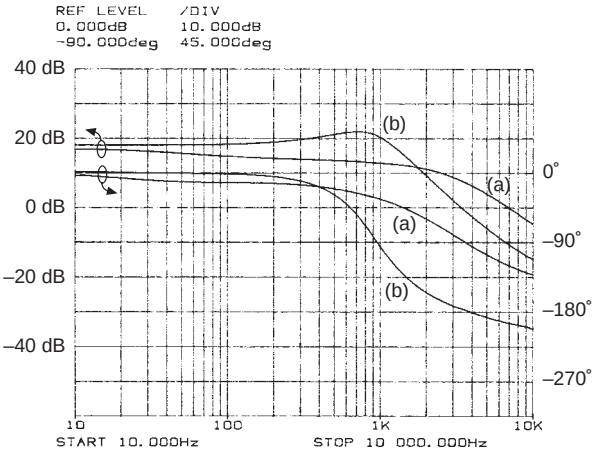

Fig. 12. Measured CCM duty-cycle-to-W_4-output magnitude and phase responses: (a) with W_2 and W_3 outputs operating in DCM, (b) with W_2 and W_3 outputs operating in CCM.

The small-signal control-to-main-output transfer function of the flyback converter was measured. The 3.3V (W_4) output was taken to be the main regulated output. The magnitude and phase of this transfer function were measured at two operating points:

(a) Both auxiliary outputs operating in discontinuous conduction mode: D = 0.515, W_2 output 13.5V at

90mA, W_3 output 14.2V at 83mA, W_4 3.4V at 0.68A.

(b) Both auxiliary outputs operating in continuous conduction mode: $D = 0.515$, W_2 output 12.1V at 2.07A, W_3 output 12.3V at 0.25A, W_4 3.4V at 0.34A.

In both cases, the 3.3V output operated in continuous conduction mode.

These dynamics were also predicted theoretically, using the automated small-signal analysis impulse-response-based approach described in [18]. The small-signal frequency response was generated by *Mathematica*, based on the converter impulse responses obtained automatically via PETS. This approach accounts for changes in operating mode of any or all of the outputs, with no input required from the user. Semiconductor conduction losses were modeled, but other nonidealities such as capacitor esr, switching loss, and flyback transformer losses, were ignored. The transformer was simulated using the *N*-port model of Fig. 7; this model is preferred because the number of inductors is equal to the number of independent states of the transformer.

The simulations converged quickly and easily, even though the system contains eight independent states. Predicted magnitude and phase responses at the two operating points are illustrated in Figs. 10 and 11. The measured small-signal response is given in Fig. 12. Agreement is quite good.

5. Conclusions

Multiple-output converters are more than simple extensions of parent single-output nonisolated converters. Imperfect coupling between windings leads to problems in cross regulation, small-signal dynamics, and multiple operating modes, which have not been fully explored in the literature. These phenomena are governed primarily by the transformer leakage inductance parameters. Hence, it is desirable to model the transformer in a way that predicts observed waveforms, that explains how converter performance depends on winding geometry, and that is useful in computer simulation.

Reduced-order geometrical models cannot predict the observed transformer waveforms for all possible excitations, and it is often difficult to predict all significant model parameters based on approximate geometrical arguments alone. A second approach, the inductance matrix, is numerically ill-conditioned in the case when the windings are well coupled. Hence, we have chosen to use a multiple-winding extension of the well-known cantilever model in this application. This model is general, each parameter can be directly measured in the laboratory, and observed waveforms can be explained using a circuit-oriented approach. Once the complete model is known, approximations can still be made (if desired), justified by measured leakage inductance parameters. The model is closely related to the inverse inductance matrix, as well as to an *N*-port model.

In the extended cantilever model, the effective turns ratios are equal to the open-circuit ratios of the winding voltages. The leakage inductance parameters are determined by driving a given winding with a voltage source, short-circuiting all other windings, and measuring the short-circuit currents. It is possible for the leakage inductance parameters to be negative; in a four-winding concentrically-wound example, a negative leakage inductance parameter arose between side-by-side windings.

A four-winding flyback transformer example proves the utility of the proposed approach. Each model parameter was measured directly. The model was checked using several other measurements; in each case, the model prediction was consistent with the measurement. The parameters of the *N*-port model were easily computed, based on the extended cantilever parameters.

The model correctly predicted observed flyback converter waveforms. The current waveform of each output winding may independently exhibit the following behaviors: discontinuous conduction mode, continuous conduction mode (with the regular negative slope), or continuous conduction mode with inverted (positive) slope. The nature of these behaviors is strongly influenced by the current slopes during the short snubber voltage clamp interval, which in turn are governed by the leakage inductance parameters. Good agreement between simulated and measured waveforms was obtained.

The model was also able to predict the converter small-signal dynamics. It was found that the control-to-output transfer function of the main output was significantly influenced by a change of operating mode in one or more auxiliary outputs. The dynamics of the three-output flyback example contain eight poles, and each output can independently operate in CCM or DCM. Nonetheless, by using the *N*-port model in conjunction with the impulse-response-based automated small-signal analysis approach, converter dynamics could be correctly modeled.

References

[1] M. Goldman and A. Witulski, "Predicting Regulation for a Multiple-Output Current-Mode Controlled DC-to-DC Converter," *IEEE Power Electronics Specialists Conference*, 1993 Record, pp.617-623.

[2] H. Matsuo, "Comparison of Multiple-Output Dc-Dc Converters Using Cross Regulation," *IEEE Power Electronics Specialists Conference*, 1979 Record, pp. 169-185, June 1979.

[3] K. Harada, T. Nabeshima, and K. Hisanaga, "State-Space Analysis of the Cross Regulation," *IEEE Power Electronics Specialists Conference*, 1979 Record, pp. 186-192, June 1979.

[4] Q. Chen, F. C. Lee, and M. Jovanovic, "Small-Signal Modeling and Analysis of Current-Mode Control for Multiple-Output Forward Converters," *IEEE Applied Power Electronics Conference*, 1994.

[5] L. Dixon, Jr., "The Effects of Leakage Inductance on Switching Power Supply Performance," Unitrode Power Supply Design Seminar, 1990, pp.P2.1-2.7.

[6] "Coupled Filter Inductors in Multiple Output Buck Regulators Provide Dramatic Performance Improvement," Unitrode Power Supply Design Seminar, 1990, pp.M7.1-7.10.

[7] D. Maksimovic, R. Erickson, and C. Griesbach, "Modeling of Cross-Regulation in Converters Containing Coupled Inductors," *IEEE Applied Power Electronics Conference*, February 1998, pp. 350-356.

[8] T. Wilson, Jr., "Cross Regulation in an Energy-Storage Dc-to-Dc Converter With Two Regulated Outputs," *IEEE Power Electronics Specialists Conference*, 1977 Record, pp. 190-199.

[9] K. Liu, "Effects of Leakage Inductances on the Cross Regulation in a Discontinuous Conduction Mode Flyback Converter," *Proceedings High Frequency Power Conversion Conference*, May 1989, pp. 254-259.

[10] S. HSU, "Problems in Analysis and Design of Switching Regulators," Ph.D. Thesis, California Institute of Technology, 1979.

[11] MIT STAFF, *Magnetic Circuits and Transformers*, Cambridge: The MIT Press, 1943.

[12] A. DAUHAJRE and R. D. MIDDLEBROOK, "Modeling and Estimation of Leakage Phenomena in Magnetic Circuits," *IEEE Power Electronics Specialists Conference*, 1986 Record, pp. 213-226.

[13] G. LUDWIG and S. EL-HAMAMSY, "Coupled Inductance and Reluctance Models of Magnetic Components," *IEEE Transactions on Power Electronics*, Vol.6, No.2, April 1991, pp. 240-250.

[14] S. CUK and Z. ZHANG, "Coupled-Inductor Analysis and Design," *IEEE Power Electronics Specialists Conference*, 1986 Record, pp. 655-665.

[15] D. HAMILL, "Lumped Equivalent Circuits of Magnetic Components: the Gyrator-Capacitor Approach," *IEEE Transactions on Power Electronics*, vol. 8, no. 2, pp. 97-103, April 1993.

[16] A. FITZGERALD, C. KINGSLEY, and S. UMANS, *Electric Machinery*, Fifth Edition, New York: McGraw-Hill, 1990.

[17] P. PEJOVIC and D. MAKSIMOVIC, "PETS—A Simulation Tool for Power Electronics," 1996 *IEEE Workshop on Computers in Power Electronics*.

[18] D. MAKSIMOVIC, "Automated Small-Signal Analysis of Switching Converters Using a General-Purpose Time-Domain Simulator," *IEEE Applied Power Electronics Conference*, February 1998, pp. 357-362.